Mechanism of Energy Coupling in the F_OF_1-ATP Synthase: The Uncoupling Mutation, γM23K, Disrupts the Use of Binding Energy To Drive Catalysis[†]

Marwan K. Al-Shawi and Robert K. Nakamoto*

Department of Molecular Physiology and Biological Physics, University of Virginia, Charlottesville, Virginia 22906-0011

Received June 20, 1997; Revised Manuscript Received August 19, 1997[⊗]

ABSTRACT: The *Escherichia coli* F_OF_1 ATP synthase uncoupling mutation, γM23K, was found to increase the energy of interaction between γ and β subunits which caused inefficient transmission of coupling information between transport and catalysis [Al-Shawi, M. K., Ketchum, C. J., and Nakamoto, R. K. (1997) *J. Biol. Chem. 272*, 2300−2306]. We hypothesized that the γM23K mutation, because of its effect on coupling, should alter the fundamental reactions steps that are normally modulated by $\Delta\mu_H+$ via the coupling mechanism. In this paper, we address this issue by studying the thermodynamics of individual catalytic steps through the use of energy profiles to gain information regarding enzyme mechanism and the effects of the mutation. Compared to wild-type enzyme, the γM23K F_1 had significant differences of two partial reactions: the rate constant for P_i release was 49-fold faster and the rate constant for ATP release was 8.4-fold faster than wild-type. These rate constants were considered together with characteristics of a group of F_1 ATPase mutant enzymes and were analyzed quantitatively by linear free energy relationships [Al-Shawi, M. K., Parsonage, D., and Senior, A. E., (1990) *J. Biol. Chem. 265*, 4402−4410]. We found that the γM23K mutation prevents the proper utilization of binding energy to drive catalysis and blocks the enzyme in a P_i release mode. This finding is consistent with the use of energy from $\Delta\mu_H+$ for increasing the affinity for P_i so that the substrate binds in a catalytically competent manner for synthesis of ATP. These results support the notion that the communication of coupling information is transmitted through the $\gamma-\beta$ interface near γMet23 and β^{380}DELSEED^{386} segment.

The F_OF_1[1] ATP synthase is a multisubunit complex that couples the movement of protons through the membranous F_O sector to the catalysis of ATP synthesis in the soluble F_1 sector. In the case of *Escherichia coli*, there are three different hydrophobic subunits in F_O with a stoichiometry of $ab_2c_{\sim 10}$, while in F_1 there are five different subunits, $\alpha_3\beta_3\gamma\delta\epsilon$. Most subunits contain conserved sequences found throughout nature especially in the catalytic domain of the complex. It is clear that the mechanism of active coupled transport is very similar in F_OF_1 ranging from archaebacteria and eubacteria to mitochondria and chloroplasts (for reviews, see refs 1−6).

Catalysis and transport mechanisms communicate indirectly by conformational linkages transmitted through a number of subunit−subunit interactions. For example, the γ and ϵ subunits, by presenting a different interface to each β subunit, impose an asymmetry that makes the β subunits structurally inequivalent and coordinates the catalytic state of each nucleotide site (*7*−*11*). Furthermore, the recently demonstrated rotation of the γ and ϵ subunits relative to the $\alpha_3\beta_3$ hexamer demonstrates that the turning movement is responsible for driving the catalytic sites through their cycles offset from each other by 120° (*12*−*15*). Mutagenesis studies have shown that residues involved in $\gamma-\beta$ interactions at the subunit−subunit interfaces and specific interactions within those interfaces are critical for not only catalytic turnover but energy coupling and complex stability as well (*16*−*19*; C. J. Ketchum, M. K. Al-Shawi, and R. K. Nakamoto, unpublished results).

One interface mutation, γM23K, has been of particular interest because it perturbs the transmission of coupling information (*20*). From the X-ray crystallographic structure of Abrahams *et al.* (*21*), we found that the ϵ-amino group of γM23K is likely to form an ionized hydrogen bond with the carboxylate of βGlu381 of the highly conserved β^{380}-DELSEED^{386} segment. Arrhenius analysis of steady-state ATP hydrolysis showed that the mutant enzyme had dramatically increased transition state enthalpic and entropic parameters (*19*). According to transition state theory, the increased thermodynamic parameters denote that an extra bond between enzyme and substrate or within the enzyme must be broken in order to achieve the transition state, hence the additional hydrogen bond created between γM23K and βGlu381. We concluded that γM23K is an added-function mutation that causes increased energy of interaction between γ and β subunits and that this is the major perturbation which causes inefficient coupling.

We hypothesized that the γM23K mutation, because of its effect on coupling, should alter the fundamental reaction steps that are normally modulated by $\Delta\mu_H+$ via the coupling mechanism. In this paper, we address this issue by studying the thermodynamics of individual catalytic steps through the use of energy profiles to gain information regarding the

[†] This work was supported by PHS grants GM50957 to R.K.N. and GM52502 to M.K.S. with additional support from National Science Foundation Grant BIR-9216996.

* Please address correspondence to Department of Molecular Physiology and Biological Physics, University of Virginia, P.O. Box 10011, Charlottesville, VA 22906-0011. Tel: (804) 982-0279. Fax: (804) 982-1616. E-mail: rkn3c@virginia.edu.

[⊗] Abstract published in *Advance ACS Abstracts,* October 1, 1997.

[1] Abbreviations: BSA, bovine serum albumin; F_1, soluble sector of the ATP synthase complex containing $\alpha_3\beta_3\gamma\delta\epsilon$; F_OF_1, the complete ATP synthase complex; γM23K, F_1 with Lys in place of subunit γMet23; LFER, linear free energy relationship; MOPS, 3-(*N*-morpholino)propanesulfonic acid; Tris, tris(hydroxymethyl)aminomethane.

S0006-2960(97)01477-3 CCC: $14.00

effects of the mutation as well as the enzyme mechanism. The characteristics of the γM23K enzyme were analyzed quantitatively with a group of F_1 ATPase mutant enzymes by linear free energy relationships (LFERs, ref 22) whose existence was previously demonstrated by Al-Shawi *et al*. (*23*). We found that the γM23K mutation prevents the proper utilization of binding energy to drive catalysis and blocks the enzyme in a P_i release mode.

EXPERIMENTAL PROCEDURES

Escherichia coli Strains and Purification of F_1. F_1 complexes were isolated from strain DK8 harboring high copy number plasmid pBWU13 (*24*) or pBMU13γM23K (*19*) and purified as described previously (*25*).

General Methods and Materials. Protein concentrations were determined by the method of Lowry *et al.* (*26*). Concentrations of ionic species of Mg^{2+}, P_i, and nucleotides were determined by the algorithm of Fabiato and Fabiato (*27*). Hexokinase (H-4502) and [2,8-^{3}H]ADP were from Sigma. [γ-^{32}P]ATP and [^{14}C]ATP were from Amersham.

Assays of Steps of Unisite Catalysis. ATP binding (k_{+1}), bound ATP hydrolysis (k_{+2}), and ATP resynthesis (k_{-2}) were measured in acid-quench/cold chase experiments as previously described (*25*). The following unisite buffer was used: 50 mM Tris-OH, 50 mM MOPS, 4.5 mM K_2SO_4, and 0.5 mM $MgSO_4$, adjusted to pH 7.5 with H_2SO_4. The final mix ratio was 0.2 μM ATP/2 μM F_1.

P_i Release (k_{+3}) and Equilibration of Bound ATP and Bound P_i (K_2). As described in Al-Shawi and Senior (*25*), these constants were determined by an equilibration experiment in which F_1 and [γ-^{32}P]ATP are mixed and bound ATP, bound P_i, and total ^{32}P are measured as a function of time. Briefly, 12.5 μL of 0.4 μM [γ-^{32}P]ATP was rapidly mixed with 12.5 μL of 4 μM or 20 μM F_1 and incubated for the required time at 23 °C. At the end of each incubation, 100 μL of unisite buffer containing 1.25 mg/mL BSA was added rapidly while vortexing for 2 s, then 100 μL of the mixture was applied to a centrifuge column and the eluate collected directly into 120 μL of 16% (w/v) $HClO_4$, 5 mM ATP, and 1 mM KH_2PO_4. Bound [γ-^{32}P]ATP, [^{32}P]P_i and experimental rate constants were determined as previously described. Since P_i release is essentially an irreversible step (*23*), the rate of P_i binding (k_{-3}) was not measured directly, rather it was calculated from the equilibrium constant for ATP hydrolysis (K_{hyd}) and the other measured rate constants as detailed in Al-Shawi and Senior (*25*).

Unisite Binding and Release of [^{3}H]ADP. Measurement of ADP dissociation (k_{+4}) and association (k_{-4}) were done as detailed previously (*28*, *29*). Various equal volume ADP/F_1 mix ratios were used and ranged from 0.5 to 4 μM final ADP concentrations with 2−10 μM final F_1 concentrations. For k_{-4} determinations, equal volumes of ADP and F_1 were rapidly mixed under unisite conditions and incubated at 23 °C for the required time, and bound nucleotide was assayed by the centrifuge column method (*30*). Alternatively, the mixture was diluted 11-fold with cold chase MgATP to give a final concentration of 5 mM ATP, 2.5 mM $MgSO_4$, and 1 mg/mL BSA in the unisite buffer. After 1 min incubation, the remaining bound noncatalytic nucleotide was determined by centrifuge column analysis. For k_{+4} determination, equal volumes of ADP and F_1 were mixed and preincubated at 23 °C for 3−6 h. The mixture was passed through a centrifuge column into a 50-fold dilution of unisite buffer containing 1 mg/mL BSA and 0.3 μM nonradioactive ADP as an isotope trap. At subsequent times, samples were analyzed for remaining bound nucleotide by centrifuge column analysis. Alternatively, samples were assayed for noncatalytic bound nucleotides by the addition of cold chase MgATP as described above.

Release of [^{14}C]ADP from Unisite Hydrolysis of [^{14}C]ATP and Release of [γ-^{32}P]ATP. Using a bent-tipped syringe for rapid mixing (*31*), 60 μL of 2 μM [^{14}C]ATP was mixed with 60 μL of 10 μM F_1 in a vortexed tube and preincubated for 2 min at 23 °C to allow unisite ATP binding. The mixture was then passed through a centrifuge column, to remove unbound nucleotide, into 2.4 mL of unisite buffer supplemented with 1 mg/mL BSA and 0.3 μM nonradioactive ADP. At various time intervals, remaining bound nucleotide was determined by centrifuge column analysis. To calculate the true k_{+4} rate, the apparent rate of [^{14}C]ADP release was multiplied by the partitioning factor ($1 + K_{-2}$) since total bound nucleotide was the sum of [^{14}C]ATP and [^{14}C]ADP bound. To determine the catalytically competent nucleotide bound, the premix was subjected to MgATP cold chase analysis as detailed above. In order to determine the release rate of ATP from the unisite, parallel experiments were done utilizing [γ-^{32}P]ATP instead of [^{14}C]ATP, and ATP release was assayed by a glucose-hexokinase trap. Briefly, the premix was incubated for 2 min as above and then passed through a centrifuge column into a 21-fold dilution of unisite buffer supplemented with 1 mg/mL BSA, 1 mg/mL hexokinase, and 100 mM glucose. After various times, 100 μL samples were removed and the reaction was stopped by the addition of 100 μL of 2 M HCl and 1 mM P_i. Analysis of glucose-6-^{32}P formation and ATP release rate (k_{-1}) were performed as described by Penefsky (*32*). Experiments utilizing a mix ratio of 0.2 μM ATP/2 μM F_1 were also done.

RESULTS AND DISCUSSION

The γM23K Mutation Does Not Alter Unisite Binding and Hydrolysis of [γ-^{32}P]ATP. We previously demonstrated that the catalytic transition state of F_OF_1-ATP synthase was very sensitive to changes in catalytic site conformation and the utilization of binding energy to drive catalysis (*23*) and that these changes could be used to probe the effects of the γM23K mutation on coupling and catalysis (*19*). Thus, we initially investigated the effects of the mutation on unisite catalysis in which catalysis occurs at a single site unencumbered by site−site cooperativity. The unisite kinetic mechanism is shown in Table 1 (*33*, *34*) and consists of the following four steps: step 1, ATP binding and release; step 2, catalytic step; step 3, P_i binding and release; and step 4, ADP binding and release. Upon addition of excess substrate, the turnover rate of the wild-type enzyme is accelerated by 7×10^4 fold (pH 7.5, 23 °C and 0.5 mM free Mg^{2+}; unisite buffer conditions, see Experimental Procedures) to attain V_{max} rates (*25*).

The pre-steady-state hydrolysis of 0.2 μM [γ-^{32}P]ATP incubated with 2 μM γM23K F_1 is shown in Figure 1. These results show that unisite ATP hydrolysis of the mutant enzyme is essentially the same as those obtained previously for wild-type F_1 (*25*). The directly acid quenched measurement assesses enzyme-bound [^{32}P]P_i plus [^{32}P]P_i released to the medium. The cold-chase result additionally measures

Table 1: Average Unisite Constants of Catalysis at pH 7.5 and 23 °C[a]

	k_{+1} (M^{-1} s^{-1})	k_{-1} (s^{-1})	K_1 (M^{-1})	k_{+2} (s^{-1})	k_{-2} (s^{-1})	K_2	k_{+3} (s^{-1})	k_{-3} (M^{-1} s^{-1})	K_3 (M)	k_{+4} (s^{-1})	k_{-4} (M^{-1} s^{-1})	K_4 (M)
WT F_1[b]	1.1×10^5	2.5×10^{-5}	4.4×10^9	1.2×10^{-1}	4.3×10^{-2}	2.9	1.2×10^{-3}	4.8×10^{-4}	2.4	1.6×10^{-3}	1.8×10^2	8.8×10^{-6}
Lys-23 F_1[c]	1.0×10^5	2.1×10^{-4}	4.8×10^8	1.2×10^{-1}	1.4×10^{-1}	0.88	5.9×10^{-2}	2.6×10^{-3}	23	7.1×10^{-3}	2.5×10^2	2.8×10^{-5}
relative fold change[d]	1.1	8.4	9.2	1.0	3.3	3.3	49	5.4	9.6	4.4	1.4	3.2

[a] Unisite hydrolysis is noncooperative ATP hydrolysis at a single β catalytic site by the following kinetic scheme (*33, 34*).

$$\begin{array}{c} \\ \uparrow \\ P_i \end{array}$$

$$F_1 + ATP \underset{k_{-1}}{\overset{k_{+1}}{\rightleftharpoons}} F_1 < ATP \underset{k_{-2}}{\overset{k_{+2}}{\rightleftharpoons}} F_1 < ADP{\cdot}P_i \underset{k_{-3}}{\overset{k_{+3}}{\rightleftharpoons}} F_1 < ADP \underset{k_{-4}}{\overset{k_{+4}}{\rightleftharpoons}} F_1 + ADP$$

[b] Wild-type F_1 values are from Al-Shawi and Senior (*25*) measured under identical conditions. [c] Averaged values from three to six experiments. [d] For ease of comparison, the numerically larger constant is divided by the smaller one.

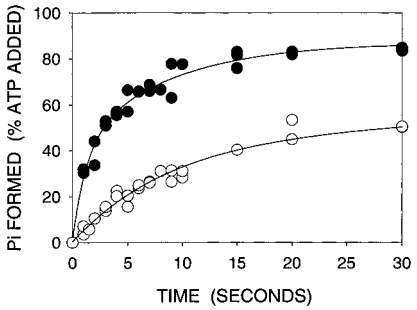

FIGURE 1: Unisite ATP hydrolysis by γM23K F_1. F_1 (12.5 μL) was vortexed with 12.5 μL of [γ-^{32}P]ATP using a 90° bent-tipped syringe such that the final concentration ratio was 0.2 μM ATP/2 μM F_1, then it was either (a) quenched with 475 μL of unisite buffer containing 1.05 mM potassium phosphate, 8.2% (w/v) $HClO_4$, 4.6 mM ATP, and 2.3 mM $MgSO_4$ (acid quench) or (b) diluted with 415 μL of unisite buffer containing 5.3 mM ATP and 2.65 mM $MgSO_4$, incubated 1 min, and then quenched with 60 μL of 65% $HClO_4$ and 8 mM potassium phosphate (cold chase). From such experiments the values of k_{+1}, k_{+2}, and k_{-2} are calculated (*28*). (●) Cold chase; (○) acid quench. The solid lines show the calculated reaction progress curves when the unisite rate equation (Table 1) is fitted with the following constants: $k_{+1} = 1.1 \times 10^5$ M^{-1} s^{-1}, $k_{+2} = 0.14$ s^{-1}, $k_{-2} = 0.15$ s^{-1} (for the data shown here) and k_{-1} and k_{-3} values from Table 1.

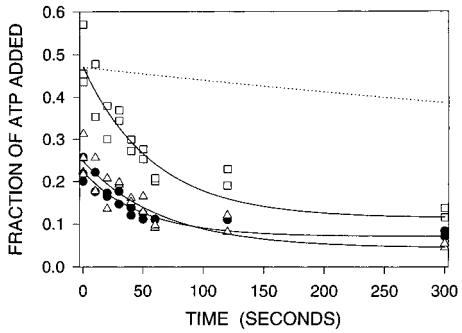

FIGURE 2: Hydrolysis and loss of γM23K F_1 bound ^{32}P species. Enzyme bound hydrolysis of [γ-^{32}P]ATP was assayed by mixing a final concentration of 0.2 μM [γ-^{32}P]ATP with 2 μM γM23K F_1 as detailed in Experimental Procedures. For the data shown here, K_2 (catalytic equilibrium constant) was 1.1 and k_{+3} (P_i off-rate) was 3.7×10^{-2} s^{-1}. (□) Total bound ^{32}P; (●) bound ATP; (△) bound P_i. The solid lines show the regressed reaction progress curves for γM23K F_1. For comparison, the dotted line shows the expected loss of total bound ^{32}P for wild-type F_1 calculated from the constants of Table 1.

[γ-^{32}P]ATP bound to F_1 and committed to hydrolysis. From this experiment, it is possible to calculate the second-order rate constant for ATP binding ($k_{+1} = 1.1 \times 10^5$ M^{-1} s^{-1}; Figure 1 and Table 1), which was very similar to wild-type F_1 (Table 1). Rate constants k_{+2} and k_{-2} for the catalytic interconversion step ($F_1 < ATP \rightleftharpoons F_1 < ADP{\cdot}P_i$) are also calculated from such experiments after the determination of k_{-1} and k_{+3} (discussed later). Again, the values of k_{+2} (0.12 s^{-1}) and k_{-2} (0.14 s^{-1}) for γM23K F_1 were similar to those of wild-type F_1 (Table 1).

The γM23K Mutation Alters Unisite P_i Release (k_{+3}). The equilibrium between bound ATP and bound P_i (K_2) and the rate of P_i release were determined in an equilibration experiment in which F_1 and [γ-^{32}P]ATP are rapidly mixed and bound ATP, bound P_i, and total ^{32}P are determined. Figure 2 shows the result of such an experiment for γM23K F_1 from which it is clear that K_2 is close to unity and similar to the value of 2.9 for wild-type F_1 (Table 1). Since the ATP release rate is slow (see below), the rate of P_i release is calculated from the rate of loss of enzyme bound ^{32}P adjusted for partitioning of bound ^{32}P between the two species $F_1 < ATP$ and $F_1 < ADP{\cdot}P_i$. Thus, the rate constant for ^{32}P loss from the enzyme is multiplied by the value of $(1 + K_{-2})$ to obtain k_{+3} since only $1/(1 + K_{-2})$ of the radioactivity bound to F_1 is present as $^{32}P_i$ ($F_1 < ADP{\cdot}P_i$) (*32*). In Figure 2, it is clear that the rate of P_i release has accelerated in the mutant enzyme compared to the wild-type form. k_{+3} was found to be 49-fold faster in the mutant enzyme (Table 1) which represents a significant change in this rate constant.

The γM23K Mutation Has Little Effect on the Binding and Release of Nucleotides. Figure 3A shows the measurement of association (k_{-4}) and dissociation (k_{+4}) rates of [^{3}H]ADP binding to a single γM23K enzyme catalytic site. After subtracting the extent of noncatalytic site ADP binding (non-ATP chaseable, Figure 3A), k_{-4} was found to be similar to wild-type (2.5×10^2 M^{-1} s^{-1}; Table 1), but k_{+4} was slightly accelerated by 4.4-fold (7.1×10^{-3} s^{-1}; Figure 3A and Table 1).

Using the mutant enzyme βY331W as a direct fluorescent probe of nucleotide binding, Weber *et al.* (*35*) found that the initial on rate for ADP binding was much faster than that seen by the centrifuge column procedure (as above). Because the K_d was not much changed, a faster off-rate is implied as well. A possible explanation for this was thought to be an initial rapid binding of ADP to the first catalytic site followed by a slower enzyme isomerization step to a new $F_1 <$ ADP conformation. This new conformation would have the slower ADP release rate measured by centrifuge column analysis. On the other hand, the on-rate measured by centrifuge column (k_{+4}) would be an apparent rate that represents the product of the true ADP on rate and the isomerization step.

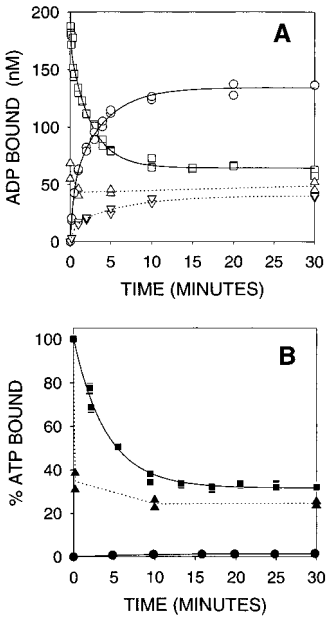

FIGURE 3: Measurement of association and dissociation rates (k_{-4} and k_{+4}) of ADP for γM23K F_1. See Experimental Procedures for details. (A) Total association of ADP with γM23K F_1 (○) was measured by mixing 0.5 μM [^{3}H]ADP with 2 μM F_1. Free ligand was removed at times indicated by a centrifuge column, and the amount of bound [^{3}H]ADP was quantitated. Noncatalytic site binding of [^{3}H]ADP (▽) was quantitated by MgATP cold chase analysis. k_{-4} was 2.8×10^2 M^{-1} s^{-1} in this experiment. Dissociation of [^{3}H]ADP from γM23K F_1 was measured using a mixture of 0.5 μM [^{3}H]ADP with 10 μM F_1 that had been preincubated for 3 h. Unbound ligand was removed, then 50-fold diluted into buffer containing 0.3 μM nonradioactive ADP as an isotope trap. Release of [^{3}H]ADP (□) was quantitated as a function of time by centrifuge column analysis. Noncatalytic site bound [^{3}H]ADP (△) was quantitated by MgATP cold chase analysis. k_{+4} was 7.1×10^{-3} s^{-1} in this experiment. (B) Dissociation of [^{14}C]ADP from γM23K F_1 after hydrolysis of [^{14}C]ATP (■) was measured by mixing 1 μM [^{14}C]ATP with 5 μM F_1. Unbound ligand was removed after 2 min and the mixture diluted 21-fold into buffer containing 0.3 μM nonradioactive ADP. Bound nucleotide was quantitated as above. (ATP bound 100%) was equivalent to 0.77 μM [^{14}C]ATP. Noncatalytic site bound [^{14}C]ATP (▲) was quantitated as described in panel A, above. Release of bound ATP (●) was determined as glucose-6-^{32}P formation in a parallel experiment using [γ-^{32}P]ATP instead of [^{14}C]ATP. [γ-^{32}P]ATP and γM23K F_1 were incubated for 2 min as above, unbound ligand was removed, and the mixture diluted 21-fold into a glucose-hexokinase trap buffer. Released ATP was trapped as glucose-6-^{32}P as a function of time. Knowing the value of K_2 for partitioning of bound nucleotide (Table 1), k_{+4} was found to be 8.5×10^{-3} s^{-1} in this experiment. Additionally, with the determined value of k_{+3} (Table 1), k_{-1} was calculated from the data shown here to be 2.0×10^{-4} s^{-1}.

In order to determine the relevant off-rate for unisite release of ADP, and hence the relevant on-rate, we measured the release of [^{14}C]ADP generated from unisite hydrolysis of [^{14}C]ATP. Figure 3B shows the rate of release of bound [^{14}C]nucleotide as well as the very small rate of release of bound ATP. After subtraction of bound nucleotide that is not chaseable by ATP (Figure 3B) and correcting for partitioning (see Experimental Procedures), the calculated k_{+4} rate was 8.5×10^{-3} s^{-1}. This was very similar to the rate of 7.1×10^{-3} s^{-1} calculated from Figure 3A for the release of [^{3}H]ADP. This determination does not require a partitioning correction since phosphate binding does not occur under unisite conditions (*28*). From the experiment of Figure 3B, it is clear that the k_{+4} and k_{-4} values of Table 1 are the relevant values for this analysis of unisite hydrolysis of ATP. Furthermore, as both the rate of release of unisite P_i (Figure 2) and ADP (Figure 3) were directly measured, it can be concluded that the turnover rate of unisite catalysis is slow.

This last conclusion is in contrast to the assertions of Reynafarje and Pedersen (*36*), who recently suggested that ATP hydrolysis by F_1-ATPase is noncooperative and that all participating catalytic sites are kinetically equivalent and exhibit Michaelis−Menton kinetics with a single K_M for ATP such that the rate of ATP hydrolysis has a first power dependence on concentration. They further propose that the unisite turnover number of 10^{-4} s^{-1} "is not an accurate reflection of the actual value" but represents an underestimate of the "true" turnover rate. There are many lines of evidence to refute these statements. The three most compelling arguments relevant to this paper are as follows. (1) Using unisite experimental conditions in which the ATP concentration was less than wild-type F_1 concentration and absolute concentrations were kept submicromolar, we found that the intrinsic unisite rate of P_i formation did not vary over a 120-fold change in the mix ratio of ATP/F_1 (*29*). This result cannot be accommodated by the model of Reynafarje and Pedersen. (2) These authors used a chemiluminescent assay that monitors ATP disappearance from the medium which they equated to the ATP hydrolytic rates. Assuming the unisite kinetic scheme (Table 1) and utilizing the rate constants determined by Grubmeyer *et al.* (*33*) for bovine heart F_1, we calculated the apparent rates of ATP removal from the medium expected in the Reynafarje and Pedersen experiments. Under expected unisite conditions (low ATP/F_1 ratios), we found a good agreement between the experimental data (Table 1 of ref 36) and our calculated expectations (<2-fold difference in all cases), supportive of the unisite scheme as originally proposed (*33*). (3) Weber *et al.* (*35*) have unequivocally demonstrated the cooperative nature of MgATP binding to the three catalytic sites by true equilibrium binding methods.

The rate of [γ-^{32}P]ATP release from γM23K F_1 was analyzed by a glucose/hexokinase trap (Figure 3B) corrected for partitioning between bound substrates and products (*34*). It was found that the slow rate of ATP release ($k_{-1} = 2.1 \times 10^{-4}$ s^{-1}; Table 1) was 8.4-fold accelerated from the wild-type value. This represents a significant change in k_{-1} by γM23K F_1.

Effects of the γM23K Mutation on Noncooperative Catalysis. In summary, the biggest effects of the γM23K mutation on unisite catalysis occur on the rate of P_i release (k_{+3}, Table 1), which is accelerated by 49-fold, followed by an 8-fold acceleration of the ATP release step (k_{-1}). Our previous analysis (*23*) has implicated these steps as energy conserving steps in the conversion of $\Delta\mu_H$+ energy into chemical conformational energy and in the conformational power stroke of the enzyme. It is also notable that γM23K did not affect the catalytic step itself (k_{+2} and k_{-2}, Table 1), implying that the chemistry of noncooperative catalysis had not changed as was predicted (see ref 19).

Effects of the γM23K Mutation on Nucleotide Binding Energy Utilization. The effects of γM23K can be analyzed quantitatively by calculation of structure−activity relationships with the linear free energy methods of Fersht *et al.* (*22*, *23*). Characteristics of a group of mutant enzymes can be analyzed quantitatively by the demonstration of the existence of linear free energy relationships (LFERs) from

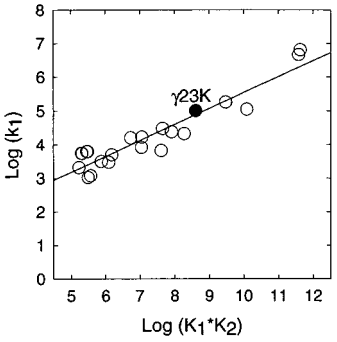

FIGURE 4: Linear free energy plot of ATP hydrolysis under unisite conditions by various F_1 enzymes. Linear free energy analysis was performed as previously described (*22*, *23*). This plot illustrates the relative relationship between binding energies achieved by the transition state for the binding and release of ATP ($K_1^{\ddagger}$) for the reaction $F_1 + ATP \rightarrow K_1^{\ddagger}$ (log k_1; *y*-axis) compared to the binding energy achieved by the enzyme intermediate ground state ($F_1 <$ ADP·P_i) for the reaction $F_1 + ATP \rightarrow F_1 <$ ADP·P_i (log K_1K_2; *x*-axis). See text for further details. To generate these plots, data obtained here was combined with data obtained previously for various β-subunit mutant enzymes, soluble bovine mitochondrial F_1, and membrane bound mitochondrial F_1 (*28*, *29*, *45*, *46*). The solid line was generated by linear least-squares regression analysis of the data ($\beta = 0.473$, $r = 0.945$).

which trends and exceptions become readily apparent (*22*, *37*). The use of binding energy to enhance catalysis is an essential feature of enzyme mechanisms (*22*, *38*, *39*). Quantitation of the use of binding energy throughout a reaction pathway can be obtained from the slopes (β values) of LFERs (*22*, *23*, *40*). By constructing the appropriate LFER plots (Figures 4 and 5) for the reaction intermediates and transition states, it was demonstrated that γM23K F_1 was indeed part of a continuum of mutant F_1 enzymes which affected catalysis through subtle structural changes that led to changes in binding energy utilization (*23*). The locations of γM23K F_1 on the regression lines of Figure 5, panels A and B, demonstrate the point above and additionally indicate that the mutation does not have a direct effect on the ground state $F_1 <$ ADP·P_i (Figure 5A) nor does it affect the catalytic transition complex $[F_1 <$ ATP$]^{\ddagger}$ directly (Figure 5B). Rather, its effect on these structures is indirect and is caused by subtle changes in the catalytic site induced by the remote mutation. The value of 1.1 for the gradient of the regression line (β value; Figure 5A) indicates that the ground state $F_1 <$ ADP·P_i achieves approximately 110% of the binding energy utilization achieved by the ground state $F_1 <$ ATP. Similarly, the catalytic transition state $[F_1 <$ ATP$]^{\ddagger}$ also achieves about 115% ($\beta = 1.15$; Figure 5B) of that achieved by the ground state $F_1 <$ ATP. Figure 5, panels A and B, are further evidence that the γM23K mutation did not cause any gross disruptive change in structure of the catalytic nucleotide binding domain.

By construction of an exhaustive set of LFER plots (not shown), we observed that the γM23K mutation had no direct effect on the structures of the enzyme intermediate ground states nor on the transition states. The exception was the transition state for the binding and release of phosphate $K_3^{\ddagger}$. In all plots in which the transition state $K_3^{\ddagger}$ was being compared to the other enzyme intermediates and transition states, it was seen that the γM23K F_1 result was displaced off the regression line (e.g., Figure 5C). In contrast, the γM23K mutation had only an indirect and proportional effect on the transition structure for ATP binding and release $K_1^{\ddagger}$ (Figure 4) even though it appeared to have a significant effect on this step when considering the kinetic data alone (Table 1). The above analysis clearly illustrates that the remote mutation γM23K was specifically changing the structure of the catalytic site transition state for the binding and release of phosphate. Since it was previously shown that the binding of P_i to the catalytic site requires energy input from $\Delta\mu_H+$ via F_O (*23*, *41*, *42*), it can be concluded that the effect of the γM23K mutation was directly in the pathway of transmission of this energy from F_O to F_1. This conclusion is valid even though the measurements were done on soluble F_1 because the perturbation caused by the mutation is the last interface of the transmission pathway between γ and β subunits.

Figure 6A shows the utilization of nucleotide binding energy by wild-type F_1 to drive the various steps of the reaction pathway in the direction of ATP synthesis. As was previously observed (*23*), maximal utilization of binding energy is achieved at the important coupling step, namely, the transition state for the binding and release of phosphate ($K_3^{\ddagger}$). A difference binding energy plot (*22*) between wild-type F_1 and γM23K F_1 is shown in Figure 6B. Clearly, the γM23K mutant enzyme must utilize more binding energy

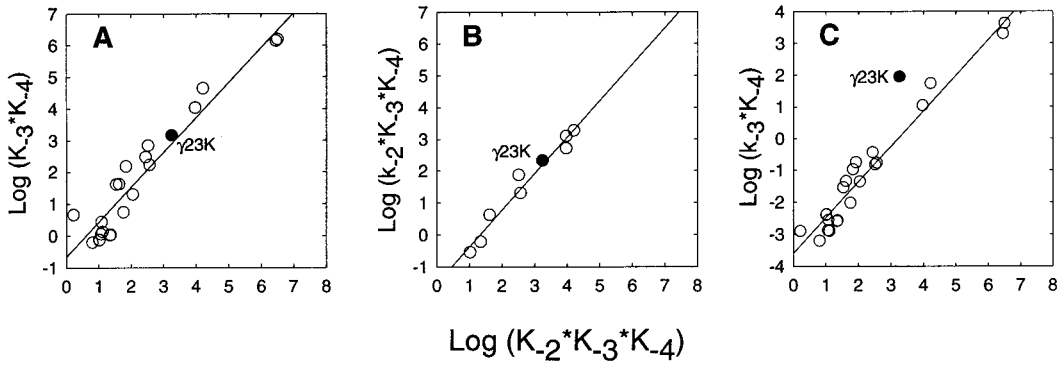

FIGURE 5: Linear free energy plots of ATP synthesis under unisite conditions by various F_1 enzymes. The plots illustrate the relative relationships between binding energies achieved by three steps of catalysis compared to the binding energy achieved by the enzyme intermediate ground state ($F_1 <$ ATP) for the reaction $F_1 + ADP + P_i \rightarrow F_1 <$ ATP [log($K_{-2}K_{-3}K_{-4}$); *x*-axis]. Data and methods employed were as given in the legend of Figure 4. See text for further details. Panel A, plot of fractional binding energy achieved by the ground state $F_1 <$ ADP·P_i for the reaction $F_1 + ADP + P_i \rightarrow F_1 <$ ADP·P_i (log($K_{-3}K_{-4}$); $\beta = 1.10$, r = 0.972]. Panel B, plot of fractional binding energy achieved by the catalytic transition state $[F_1 <$ ATP$]^{\ddagger}$ by mutations not directly involved in the chemistry of catalysis for the reaction $F_1 + ADP + P_i \rightarrow [F_1 <$ ATP$]^{\ddagger}$ [log($k_{-2}K_{-3}K_{-4}$); $\beta = 1.15$, $r = 0.982$]. Panel C, plot of fractional binding energy achieved by the transition state for P_i binding and release $K_3^{\ddagger}$ for the reaction $F_1 + ADP + P_i \rightarrow K_3^{\ddagger}$ [log($k_{-3}K_{-4}$); $\beta = 1.12$, $r = 0.985$]. Lines were fitted by linear least-squares regression analysis.

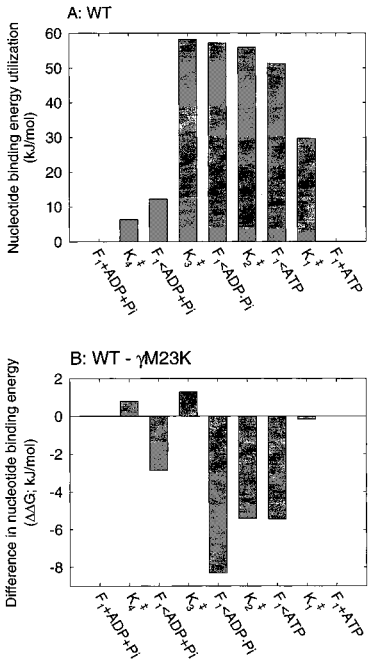

FIGURE 6: Nucleotide binding energies achieved during ATP synthesis in unisite catalysis. Panel A, nucleotide binding energy utilization by wild-type F_1 used to drive catalysis is shown for the various reaction intermediates during ATP synthesis. To generate this plot, the relative binding energies of the various reaction steps were calculated from the relevant LFERs, of the type shown in Figures 4 and 5, according to published procedures (*22*, *23*). The fractional relative binding energies were then converted into units of energy (kilojoules per mole) by normalizing the relative binding energies to the calculated ground state binding energy of $F_1 <$ ADP·P_i which was −57.2 kJ/mol for the standard states of pH 7.5, 1 M for ATP, P_i and ADP having defined $G_{F1} = 0$ (*28*). Panel B, plot of differential binding energy diagram between the wild-type F_1 and γM23K F_1 for the various reaction steps of ATP synthesis. This plot was calculated according to published procedures (*22*, *28*). Here the nucleotide binding energy utilization of wild-type F_1 was subtracted from the corresponding values of γM23K F_1 such that a loss in binding energy utilization by γM23K F_1 leads to a negative value.

to bind the substrates ADP and P_i ($K_4^{\ddagger}$ and $K_3^{\ddagger}$ of Figure 6B), which leaves a deficit of available binding energy to be used to drive ATP synthesis ($K_2^{\ddagger}$ of Figure 6B).

Significance for Structures Involved in Coupling. We previously predicted that the uncoupling mutation, γM23K, would not affect the basic catalytic mechanism but would affect the catalytic steps that are modulated by the linkage to transport (*19*). From the unisite analysis, we found that the γM23K mutant F_1 had normal unisite binding and hydrolysis of ATP, and only slightly altered unisite binding and release of ADP. Clearly, the major effect of the mutation was to increase rates of unisite release of P_i and to a lesser extent ATP. Most importantly, both steps are energy-conserving steps and indicate that the mutation perturbs the ability of enzyme to efficiently utilize binding energy to drive catalysis. Because this analysis was done in unisite conditions, it is apparent that the γM23K mutation has direct perturbations on the fundamental mechanism of catalysis. The enzyme gets stuck in a P_i release mode and is not able to achieve the optimal catalytic site conformation to carry out the chemistry of synthesis/hydrolysis (K_2). This analysis suggests that the γM23K mutation with its interaction with the β^{380}DELSEED^{386} segment breaks the transmission of coupling information by interfering with the proper position of the β^{380}DELSEED^{386} segment and, therefore, the proper configuration of the catalytic site. We suggest that the helical loop of the β subunit, which includes the β^{380}DELSEED^{386} segment, dictates, at least in part, the conformation of the catalytic site during its cycle. This notion is consistent with the crystallographic structure of Abrahams et al. (*21*) and chemical modification studies of the β^{380}DELSEED^{386} segment (*7*−*13*, *43*, *44*).

REFERENCES

1. Penefsky, H. S., and Cross, R. L. (1991) *Adv. Enzymol. 64*, 173−213.
2. Capaldi, R. A., Aggeler, R., Turina, P., and Wilkens, S. (1994) *Trends Biol. Sci. 19*, 284−289.
3. Fillingame, R. H., Girvin, M. E., and Zhang, Y. (1995) *Biochem. Soc. Trans. 23*, 760−766.
4. Deckers-Hebestreit, G., and Altendorf, K. (1996) *Annu. Rev. Microbiol. 50*, 791−824.
5. Nakamoto, R. K. (1996) *J. Membr. Biol. 151*, 101−111.
6. Weber, J., and Senior, A. E. (1997) *Biochim. Biophys. Acta 1319*, 19−58.
7. Abrahams, J. P., Buchanan, S. K., van Raaij, M. J., Fearnley, I. M., Leslie, A. G. W., and Walker, J. E. (1996) *Proc. Natl. Acad. Sci. U.S.A. 93*, 9420−9424.
8. Haughton, M. A., and Capaldi, R. A. (1995) *J. Biol. Chem. 270*, 20568−20574.
9. Kaibara, C., Matsui, T., Hisabori, T., and Yoshida, M. (1996) *J. Biol. Chem. 271*, 2433−2438.
10. Grüber, G., and Capaldi, R. A. (1996) *Biochemistry 35*, 3875−3879.
11. Grüber, G., and Capaldi, R. A. (1996) *J. Biol. Chem. 271*, 32623−32628.
12. Duncan, T. M., Bulygin, V. V., Zhou, Y., Hutcheon, M. L., and Cross, R. L. (1995) *Proc. Natl. Acad. Sci. U.S.A. 92*, 10964−10968.
13. Zhou, Y., Duncan, T. M., Bulygin, V. V., Hutcheon, M. L., and Cross, R. L. (1996) *Biochim. Biophys. Acta 1275*, 96−100.
14. Sabbert, D., Engelbrecht, S., and Junge, W. (1996) *Nature (London) 381*, 623−625.
15. Noji, H., Yasuda, R., Yoshida, M., and Kinosita, K. (1997) *Nature (London) 386*, 299−302.
16. Nakamoto, R. K., Maeda, M., and Futai, M. (1993) *J. Biol. Chem. 268*, 867−872.
17. Jeanteur-De Beukelaer, C., Omote, H., Iwamoto-Kihara, A., Maeda, M., and Futai, M. (1995) *J. Biol. Chem. 270*, 22850−22854.
18. Nakamoto, R. K., Al-Shawi, M. K., and Futai, M. (1995) *J. Biol. Chem. 270*, 14042−14046.
19. Al-Shawi, M. K., Ketchum, C. J., and Nakamoto, R. K. (1997) *J. Biol. Chem. 272*, 2300−2306.
20. Shin, K., Nakamoto, R. K., Maeda, M., and Futai, M. (1992) *J. Biol. Chem. 267*, 20835−20839.
21. Abrahams, J. P., Leslie, A. G. W., Lutter, R., and Walker, J. E. (1994) *Nature (London) 370*, 621−628.
22. Fersht, A. R., Leatherbarrow, R. J., and Wells, T. N. (1987) *Biochemistry 26*, 6030−6038.
23. Al-Shawi, M. K., Parsonage, D., and Senior, A. E. (1990) *J. Biol. Chem. 265*, 4402−4410.
24. Moriyama, Y., Iwamoto, A., Hanada, H., Maeda, M., and Futai, M. (1991) *J. Biol. Chem. 266*, 22141−22146.
25. Al-Shawi, M. K., and Senior, A. E. (1992) *Biochemistry 31*, 878−885.
26. Lowry, O. H., Rosebrough, N. J., Farr, A. C., and Randall, R. J. (1951) *J. Biol. Chem. 193*, 265−275.
27. Fabiato, A., and Fabiato, F. (1979) *J. Physiol. (Paris) 75*, 463−505.
28. Al-Shawi, M. K., and Senior, A. E. (1988) *J. Biol. Chem. 263*, 19640−19648.
29. Al-Shawi, M. K., Parsonage, D., and Senior, A. E. (1989) *J. Biol. Chem. 264*, 15376−15383.
30. Penefsky, H. S. (1979) *Methods Enzymol. 56*, 527−530.

31. Ray, W. J., and Long, J. W. (1976) *Biochemistry 15*, 3990−3993.
32. Penefsky, H. S. (1986) *Methods Enzymol. 126*, 608−618.
33. Grubmeyer, C., Cross, R. L., and Penefsky, H. S. (1982) *J. Biol. Chem. 257*, 12092−12100.
34. Duncan, T. M., and Senior, A. E. (1985) *J. Biol. Chem. 260*, 4901−4907.
35. Weber, J., Wilke-Mounts, S., Lee, R. S.-F., Grell, E., and Senior, A. E. (1993) *J. Biol. Chem. 268*, 20126−20133.
36. Reynafarje, B. D., and Pedersen, P. L. (1996) *J. Biol. Chem. 271*, 32546−32550.
37. Benkovic, S. J., Fierke, C. A., and Naylor, A. M. (1988) *Science 239*, 1105−1110.
38. Albery, W. J., and Knowles, J. R. (1976) *Biochemistry 15*, 5627−5631.
39. Albery, W. J., and Knowles, J. R. (1976) *Biochemistry 15*, 5631−5640.
40. Fersht, A. R., Leatherbarrow, R. J., and Wells, T. N. C. (1986) *Trends Biochem. Sci. 11*, 321−325.
41. Gräber, P., and Labahn, A. (1992) *J. Bioenerg. Biomembr. 24*, 493−497.
42. Fischer, S., Etzold, C., Turina, P., Deckers-Hebestreit, G., and Altendorf, K. (1994) *Eur. J. Biochem. 225*, 167−172.
43. Bullough, D. A., Ceccarelli, E. A., Roise, D., and Allison, W. S. (1989) *Biochim. Biophys. Acta 975*, 377−383.
44. Bullough, D. A., Ceccarelli, E. A., Verburg, J. G., Allison, W. S. (1989) *J. Biol. Chem. 264*, 9155−9163.
45. Senior, A. E., and Al-Shawi, M. K. (1992) *J. Biol. Chem. 267*, 21471−21478.
46. Senior, A. E., Wilke-Mounts, S., and Al-Shawi, M. K. (1993) *J. Biol. Chem. 268*, 6989−6994.

BI971477Z